REPORT DOCUMENTATION PAGE

Form Approved
OMB NO. 0704-0188

1. AGENCY USE ONLY (Leave Blank)	2. REPORT DATE 6/30/98	3. REPORT TYPE AND DATES COVERED Annual Performance: 4/1/97-3/31/98

4. TITLE AND SUBTITLE
Analysis and Optimization of Oxidized Heterolayers

5. FUNDING NUMBERS
N00014-97-1-0335

6. AUTHOR(S)
E. Weber

7. PERFORMING ORGANIZATION NAME(S) AND ADDRESS(ES)
University of California, Berkeley, CA 94720

8. PERFORMING ORGANIZATION REPORT NUMBER
442427-23086

9. SPONSORING / MONITORING AGENCY NAME(S) AND ADDRESS(ES)
Office of Naval Research / ONR 312
Ballston Centre Tower One
800 North Quincy Street
Arlington, VA 22217-5660

10. SPONSORING / MONITORING AGENCY REPORT NUMBER

11. SUPPLEMENTARY NOTES
N/A

12 a. DISTRIBUTION / AVAILABILITY STATEMENT
Approved for public release; distribution unlimited.

12 b. DISTRIBUTION CODE

13. ABSTRACT (Maximum 200 words)

The objective of this project is to develop a controlled oxidation process with minimized degradation of the adjacent device structures. A systematic study of the fundamental properties of the wet thermal oxides is being performed, including the dependence on oxide processing parameters, hydrogen and other dopant concentrations, oxidized layer thickness, and Ga concentration. The study was based on state-of-the-art structural analysis by transmission electron microscopy techniques, including structural microanalysis of the layers with respect to the phases formed and the presence of inhomogeneities.

14. SUBJECT TERMS			15. NUMBER OF PAGES 23
			16. PRICE CODE
17. SECURITY CLASSIFICATION OR REPORT **UNCLASSIFIED**	18. SECURITY CLASSIFICATION ON THIS PAGE **UNCLASSIFIED**	19. SECURITY CLASSIFICATION OF ABSTRACT **UNCLASSIFIED**	20. LIMITATION OF ABSTRACT **UL**

NSN 7540-01-280-5500
Form 298 (Rev.2-89)
Prescribed by ANSI Std. 239-18
Standard

ANALYSIS AND OPTIMIZATION OF OXIDIZED HETEROLAYERS

Principal Investigator:

Eicke R. Weber

Department of Materials Science, UC Berkeley

Co-investigators:

Zuzanna Liliental-Weber

Lawrence Berkeley National Laboratory

and

Connie Chang-Hasnain

Department of Electrical Engineering and Computer Science, UC Berkeley

INTRODUCTION

Difficulties in the formation of high-quality stable native oxides on the III-V compounds have hindered development of III-V integrated circuits and optoelectronic technology. Recently it was shown[1,2] that stable oxides can be formed on III-V compounds rich in Al, such as $Al_xGa_{1-x}As$, similar to Si technology, by reaction of $Al_xGa_{1-x}As$ with H_2O vapor at elevated temperatures (~400-450°C).[1-8] Lateral oxidation of (Ga,Al)As layers is a very attractive technology for the fabrication of isolating Al-rich oxide layers in optoelectronics because of their stability, high resistivity and near-planar topology. Therefore, this technology has been used for the fabrication of semiconductor lasers, and, recently, for vertical cavity surface emitting lasers (VCSELS).[8-12]

A typical VCSEL structure consists of a three quantum well active region sandwiched between two distributed Bragg reflectors (DBRs) as shown in (Fig 1). The lateral oxidation of the Al-rich layers in the Bragg reflectors of the VCSEL leads to the formation of oxide apertures. The AlAs layer has an eye-shaped cross-section, due to anisotropy of the vertical wet etch. The AlAs layer was then selectively oxidized from the sidewalls until a ~4 μm wide current funneling region was left. In this way, the oxidized layer confines the current injection and the optical emission to the 4μm diameter central region. The smaller refractive index of the oxide layers provides an excellent index-guided optical confinement of carriers and, as a result, leads to low threshold current and high lasing efficiency of these devices.[8-11] The presence of strain in the oxidized layers seems to cause a high degree of optical polarization of the light output.

Stable native oxides of GaAs and AlGaAs have also been used in forming self-aligned dielectric layers in the fabrication of semiconductor laser diodes,[8-9] for preventing impurity diffusion,[10] and for the fabrication of native-oxide-defined strip geometry quantum well

heterostructure laser diodes[11] as well as to enhance lateral oxidation at p-n junctions.[12]

Recent reports indicate that oxidation of an AlAs layer in water is sensitive to the temperature and growth history.[13-14] It was shown that linear growth takes place which converts to parabolic with increasing oxide thickness. It has not been clarified whether the excess As created in this process has any role in the stabilization of these oxides, in reducing leakage current or in impurity diffusion. Moreover there is concern as to the quality of the oxide/GaAs interfaces created by lateral oxidation of an intermediate AlGaAs layer.

OBJECTIVE

The objective of this project is to develop a controlled oxidation process with minimized degradation of the adjacent device structures. A systematic study of the fundamental properties of the wet thermal oxides is being performed, including the dependence on oxide processing parameters, hydrogen and other dopant concentrations, oxidized layer thickness, and Ga concentration. The study was based on state-of-the-art structural analysis by transmission electron microscopy techniques, including structural microanalysis of the layers with respect to the phases formed and the presence of inhomogeneities.

EXPERIMENTAL

The first part of the study was determination of oxidation rate on the thickness of the AlAs layer. In this part of the project different thicknesses of AlAs layers were grown. Two sets of samples were grown. One contained 7 layers of AlAs with thicknesses of 20 nm, 10 nm, 5 nm, 2.5 nm, 5 nm, 10 nm and 20 nm separated by 50 nm of GaAs with a 500 nm top layer of GaAs (sample 90B-Fig. 2a). The second set also contained 7 layers of AlAs with thicknesses of 60 nm, 45 nm, 30 nm, 15 nm, 30 nm, 45 nm, and 60 nm separated by 50 nm of GaAs

with a 50 nm top layer of GaAs (sample 91B-Fig. 2b). These samples were patterned and mesas were formed. The oxidation was carried out in a quartz furnace at 450°C in H_2O:N_2 by bubbling nitrogen through de-ionized water at 95°C. This process resulted in lateral oxidation of the AlAs layers. The oxidation was performed for either 8 min or 12 min to observe the dependence of oxidation rate on layer thickness.

The experimental mesas were prepared as strips along <110> directions. The mesas contained oxide apertures that had larger internal diameters than those usually used in devices in order to be more easily observed by TEM. The oxidized AlAs layer has a different refractive index and is amorphous, therefore the oxidation terminus can be easily observed.

Cross-section TEM samples were prepared perpendicular to the strip direction. The samples were mechanically polished followed by ion milling. Immediately after obtaining electron transparent samples TEM observation was performed to avoid any damage due to storage in the atmosphere. A Topcon 002B electron microscope with acceleration voltage of 200 KeV and point-to-point resolution 1.8 Å was used for these studies.

RESULTS

Oxidation started from the mesa's walls. High resolution TEM analysis of the as-deposited layers showed perfect crystallinity with near-atomically flat interfaces (Fig. 3). Careful adjustment of the oxidation time allows study of the lateral oxidation front. Upon oxidation the AlAs layer was transformed to γ-Al_2O_3 , as confirmed by TEM (Fig. 4). Selective area diffraction patterns obtained from the oxidized AlAs layers gave ring diffraction consistent with the following interplanar distances: 4.5, 2.78, 2.41, 1.97, 1.52, 1.4, 1.1776, and 1.138 Å. Three of these rings (2.41, 2.02 and 1.41 Å) were detected earlier[2] and were assigned to one of the phases of AlO(OH) mixed with one of the four (η,γ, χ, and δ) Al_2O_3 oxides. Taking

into account all the rings and their intensities it appears that these interplanar distances agree well with the γ-Al_2O_3 oxides.[17-20] However, at this point it is difficult to positively eliminate the presence of some pure Al in these oxide layers since interplanar distances in Al overlap with the oxides. High resolution micrographs give a hint of the presence of some small Al grains embedded in the oxides. In addition to the ring pattern small arcs containing defined spots consistent with AlAs and As could be detected as well.

Clear dependence of oxidation rate on the AlAs layer thickness was observed. For the layers with nominal thickness of 60nm, 45nm, 30nm and 15 nm (mirror structures) the difference in oxidation rate is not so drastic, and is not linear with thickness (Fig. 5). The highest oxidation rate was observed for the 30 nm thick layer. For the layers with the thickness ranging from 20 nm to 2.5 nm an almost liner dependence was observed.

The second observation was that layers closer to the sample surface oxidized slightly slower than layers closer to the substrate for the sample 91B with larger AlAs layer thickness (Fig. 2b). For the smaller layer thickness (sample 90B) the behavior was reversed (Fig. 6). It is not clear at this point if this is an influence of the sample surface or of slight differences in the layer thickness measured by high resolution electron microscopy , between nominally identical layers.

The third observation was that the oxidation process consumed more than the intended AlAs layer, since the oxidized part of the layer is slightly thicker than the unoxidized part. The oxidation reaction results in the production of excess As that is clearly visible in the form of precipitates near the oxidized layers (Fig. 7). It is expected that during the oxidation process the following reaction would take place:

$$2\,AlAs + 3\,H_2O \rightarrow Al_2O_3 + 2\,AsH_3$$

By formation of AsH_3 the samples would be depleted in As. However, the transport of excess As via the vapor phase seems not to be complete, as an accumulation of As was always

observed *inside* the structure: at the interfaces with the oxidized layers, on the top surface of the structure and as precipitates in the surrounding GaAs. This suggests a high diffusivity of As atoms or its complexes during the oxidation. The presence of As precipitates at the interfaces with oxidized layers and in the GaAs separation layers (Fig. 7) confirms that the excess As diffused through the structure rather than via the gas phase. Accumulation of this As can lead to stress close to the oxidation front which results in the formation of interfacial defects such as stacking faults (Fig. 6). Depending on the oxidation time GaAs rich in As can be formed due to As outdiffusion. The released As can diffuse through the surrounding layers towards the surface of the structure. This can be deleterious to device applications. Although this finding was originally controversial, our work has resulted in general recognition of this problem. The current work is aimed at designing structures and processing conditions to minimize the detrimental effects of oxidation for device operation.

The oxidation front has a specific asymmetric shape with the moving front at the upper interface slightly ahead of that at the lower interface. This remains true independently on the layer thickness. Figures 8-10 show oxidation front for the AlAs layers located closer and further from the sample surface. In the areas close to the oxidation front no voids can be observed. However, further back from the oxidation front, where the layer was oxidized earlier, voids are formed especially at the lower interface (Fig. 7). This void formation was observed to occur independent of the layer thickness (Fig. 11). At this point it is not clear what is responsible for void formation-longer exposure to the vapor or high temperature. Work is in progress on the annealing of these layers to see if longer exposure to high temperature can lead to void formation. Such findings are very important since formation of voids on these interfaces can weaken the structural integrity of the devices and delaminate particular layers.

CONCLUSIONS

The detailed structural characterization of wet oxidation of AlAs layers by transmission electron microscopy showed that dense γ-Al_2O_3 oxide was formed as the result of wet oxidation. As the result of the oxidation accumulation of As at the interfaces and in the GaAs surrounding the oxidized layers was observed. The oxidation front is not symmetric showing faster motion at the upper interface than at the lower interface. Clear dependence of oxidation rate on the AlAs layer thickness was observed. Only for specific layer thicknesses was a linear dependence of oxidation rate on thickness observed. In the areas some distance back from the oxidation front voids were formed at the interfaces. These voids were mostly located at the lower interface.

FUTURE WORK

In the next part of this project dependence of oxidation rate on layer composition will be studied. Ga will be added to AlAs to control the oxidation rate. Electrical measurements will accompany the structural studies. The main work will concentrate on development an oxidation process that avoids formation of voids and decreases As accumulation at the interfaces and the sample surface.

FIGURE CAPTIONS:

Fig. 1. Schematic of an oxide confined VCSEL

Fig. 2. TEM micrograph showing oxidation of AlAs layers. (a) Sample 90B with the layer thickness of 20 nm, 10 nm, 5 nm, 2.5 nm, 5 nm, 10 nm and 20 nm separated by 50 nm of GaAs; (b) Sample 91B with the layer thickness of 60 nm, 45 nm, 30 nm, 15 nm, 30 nm, 45 nm, and 60 nm separated by 50 nm of GaAs.

Fig. 3. High resolution TEM micrograph of an as-deposited AlAs layer demonstrating excellent interfacial quality.

Fig. 4. Diffraction pattern from an oxidized layer.

Fig. 5. Oxidation fronts of the AlAs layers in the sample 91B (larger thicknesses). Note dark contrast from As accumulation at the oxidized interfaces (only lower part of the sample closer to the substrate is shown).

Fig. 6. An oxidation front in the 20 nm AlAs layers located closer and further from the substrate. Note accumulation of As at the interfaces with the oxidized layers and formation of stacking fault close to the oxidation front in the upper layer.

Fig. 7. This micrograph shows the oxidation process of the 20 nm thick AlAs layer (at the bottom of this micrograph) than in the 10 nm layer above. Formation of voids at the lower interface is visible. As accumulation between the two oxidized layers is similar to low-temperature grown GaAs after annealing. Note the formation of As precipitates between the oxidized layers. Oxidation fronts for AlAs layers with smaller thicknesses is much behind the 10 nm thick layer and is not visible on this micrograph.

Fig. 8. An oxidation front in the layer with a nominal thickness of 30 nm (slightly smaller thickness was measured by high resolution TEM) located closer to the sample surface.

Fig. 9. An oxidation front in the layer with a nominal thickness of 30 nm (slightly smaller thickness was measured by high resolution TEM) located closer to the substrate.

Fig. 10. An oxidation front in the layer with a nominal thickness of 45 nm (slightly smaller thickness was measured by high resolution TEM) located closer to the sample surface. Note the same shape of the oxidation front.

Fig. 11. Oxidized layer with the nominal thickness of 15 nm at the mesa edge. Note larger undulation of the lower interface suggesting void formation.

Fig. 12. Oxidized layer with the nominal thickness of 30 nm at the mesa edge. Note larger undulation of the lower interface suggesting void formation.

REFERENCES

1. A.R. Sugg, N. Holonyak, Jr., J.E. Baker, F.A. Kish, and J.M. Dallesasse, Appl. Phys. Lett., **58**, 1199 (1991).
2. A.R. Sugg, E.I. Cnen, N. Holonyak, Jr., K.C. Hsieh, J.E. Baker, and N. Finnegan, J. Appl. Phys., **74**, 3880 (1993).
3. G. S. Li, S. F. Lim, W. Yuen and C. J. Chang-Hasnain, Electronics Letters., **31**, 23, pp. 2014-5, 1995.
4. D. L. Huffaker, J. Shin, and D. G. Deppe, Electron. Lett., **30**, 1946 (1994).
5. K.L. Lear, K.D. Choquette, R.P. Schneider, JR., S.P. Kilcoyne, and K.M. Geib, Electron. Lett., **31**, 208 (1995).
6. M.H. Macdougal, P.D. Dapkus, V. Pudikov, Z. Hanmin, and Y. Gye Mo, IEEE Photonics Technol. Lett., **7**, 229 (1995).
7. A.R. Sugg, N. Holonyak, Jr., J.E. Baker, F.A. Kish, and J.M. Dallesasse, Appl. Phys. Lett., **50**, 1199 (1991).
8. D.D. Liu, B. Zhang, D.H. Wang, and W.X. Chen, Appl. Phys. Lett. **38**, 557 (1981).
9. A. Kurobe, H. Furuyama, S. Naritsuka, Y. Kokubun, and M. Nakamura, Electron. Lett. **22**, L118 (1986).
10. 5.J.M. Dellesasse, N. Holonyak, Jr, N. El-Zein, T.A. Richard, F.A. Kish, A.R. Sugg, R.D. Burnham, and S.C. Smith, Appl. Phys. Lett., **58**, 974 (1991).
11. F.A. Kish, S.J. Caracci, S.A. Maranowski, N. Holonyak, Jr. S.C. Smith, and R.D. Burnham, Appl. Phys. Lett, **60**, 1582 (1992).
12. S.A. Maranowski, N. Holonyak Jr. T.A. Richard, and F.A. Kish, Appl. Phys. Lett., **62**, 2087 (1993).
13. M.Ochiai, G.E. Giudice, H. Temkin, J.W. Scott, T.M. Cockerill, Appl.Phys.Lett., **68**, 1898 (1996).
14. K.D. Choquette, K.M. Geib, H.C. Chui, H.Q. Hou, R. Hull, Mat. Res. Soc.

17. S. Guha, F. Agahi, B. Pezeshi, J.A. Kash, D.W. Kisker, and N.A. Bojarczuk, Appl. Phys. Lett., 68, 906 (1996).

18. Z. Liliental-Weber, M. Li, G.S. Li, C. Chang-Hasnain, and E.R. Weber, *in Proceedings of Microscopy and Microanalysis*, edts. G.W. Bailey, J.M. Corbet, R.V.W. Dimlich, J.R. Michael, and N.J. Zaluzec, San-Francisco Press.,San Francisco, (1996), p.942.

19. Z. Liliental-Weber, M. Li, G.S. Li, C. Chang-Hasnain, and E.R. Weber,in "Semi-isulating III-V Materials,"Toulouse, France, April 1996 in print.

20. Z. Liliental-Weber, S. Ruvimov, W. Swider, J. Washburn, M. Li, G.S. Li, and C. Chang-Hasnain, and E.R. Weber, "Al-based thermal oxides in vertical cavity surface emitting lasers, " SPIE-The International Society for Optical Engineering Proceedings, **3006**. 15 (1997).

Schematic of an Oxide Confined VCSEL

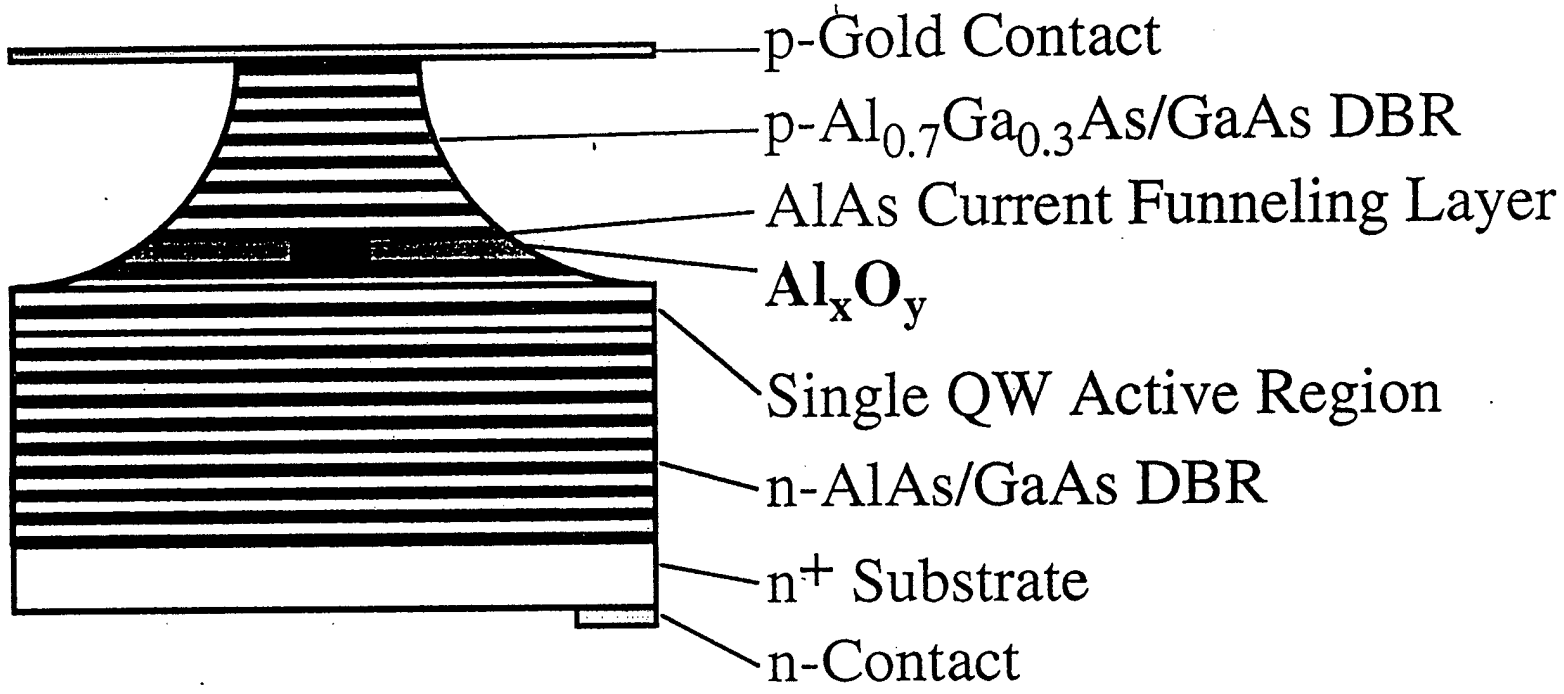

Fig. 1

- AlxOy provides electrical and optical confinement.

Connie Chang-Hasnain Group

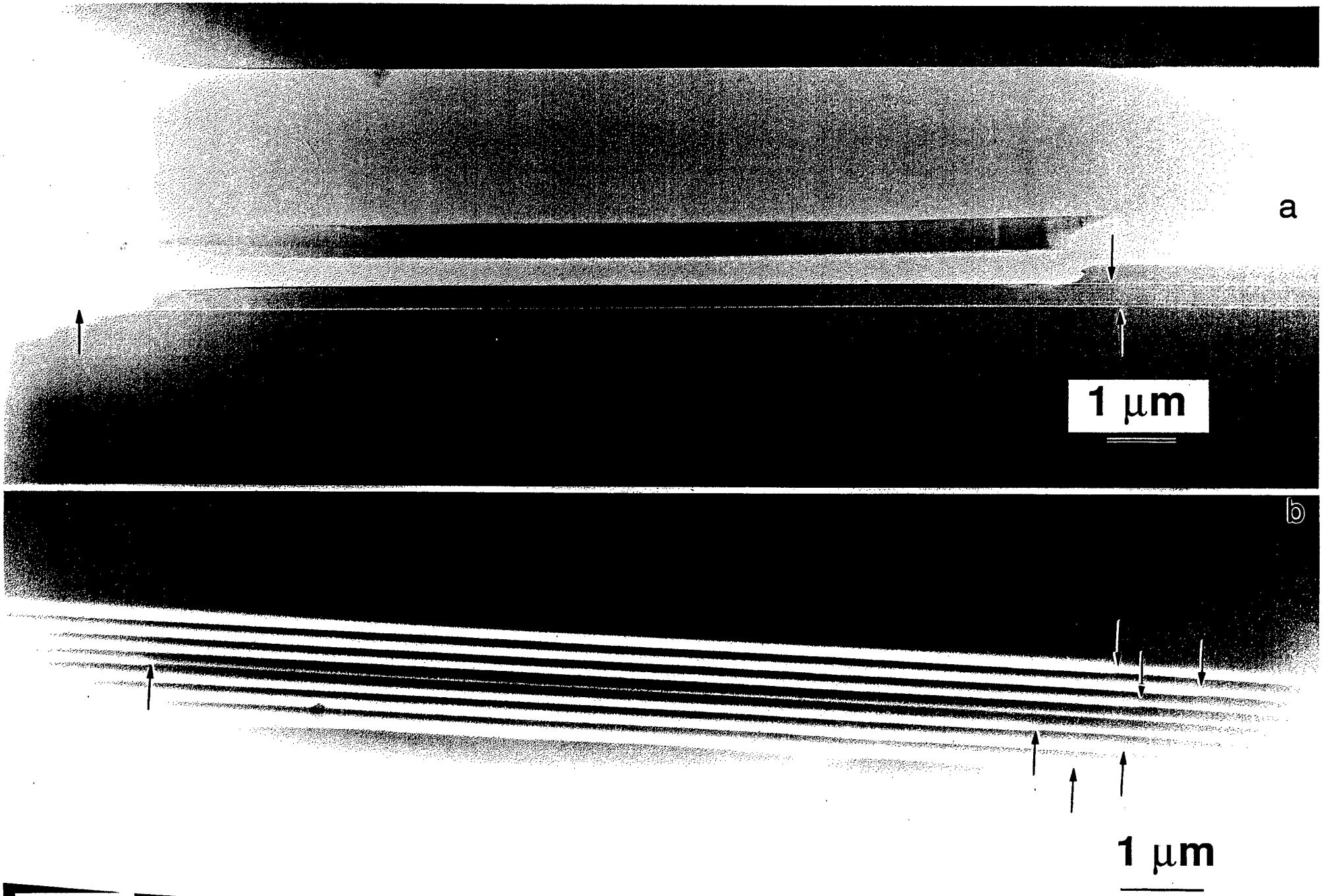

Fig. 2

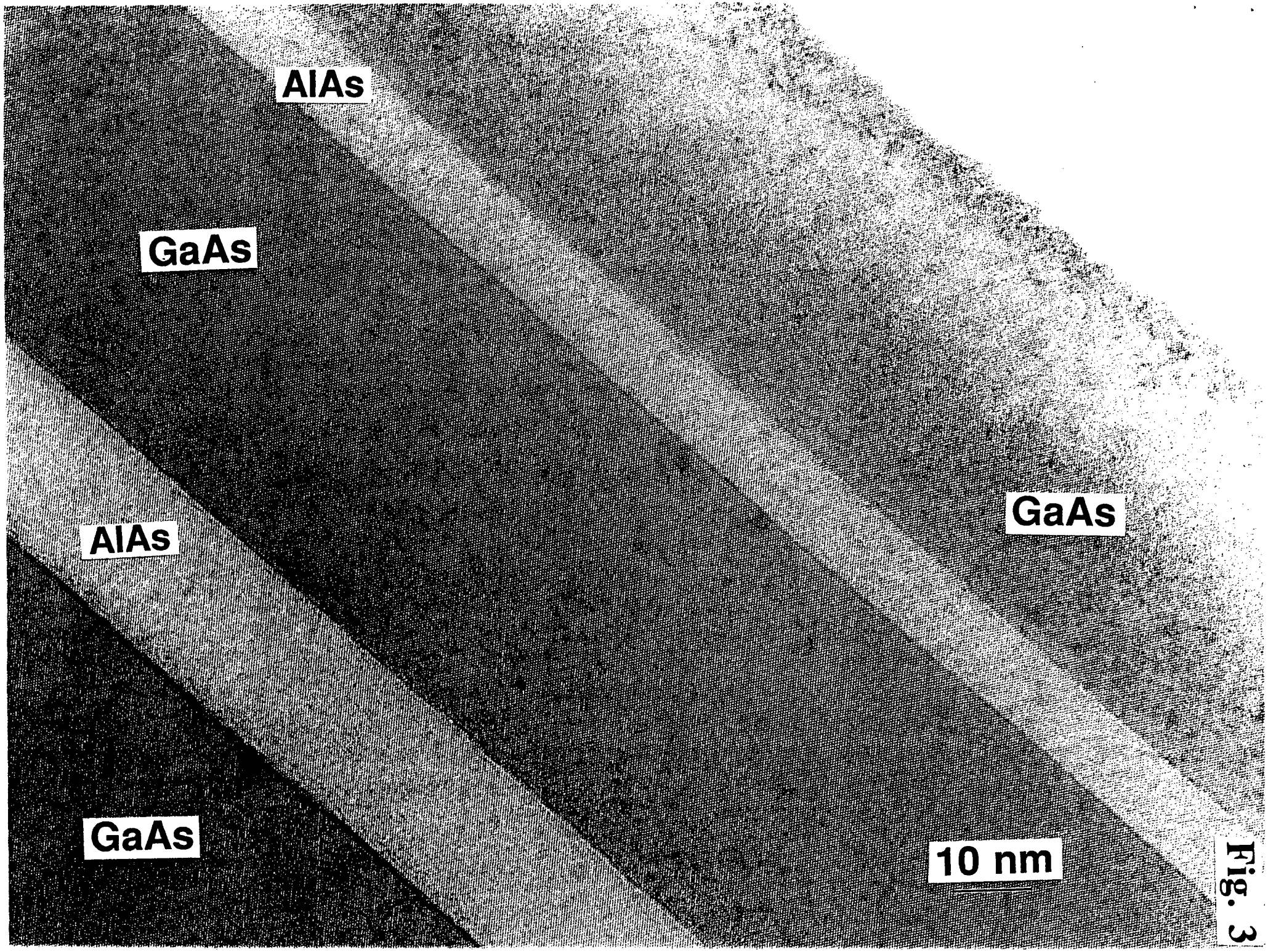

Fig. 3

Fig. 4

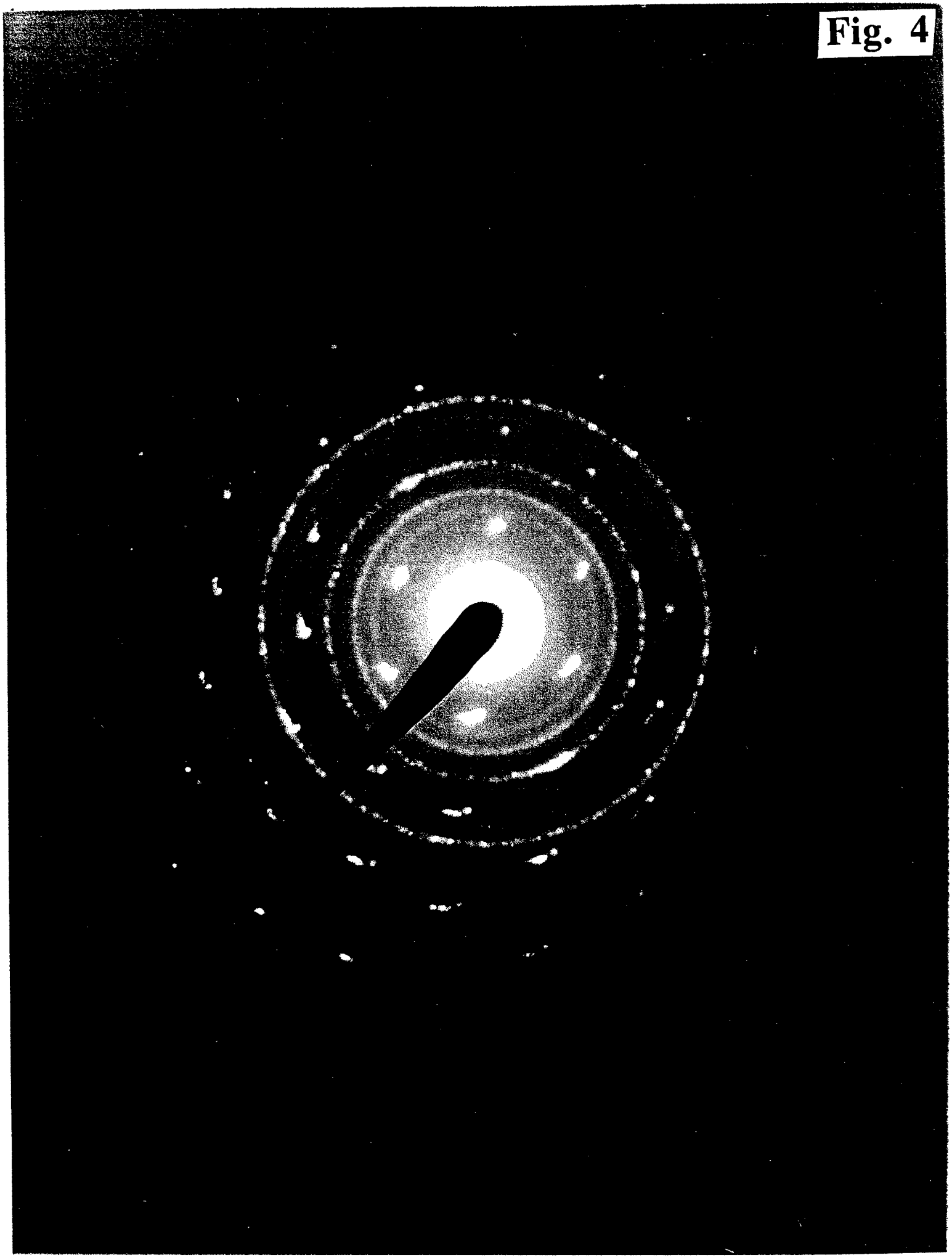

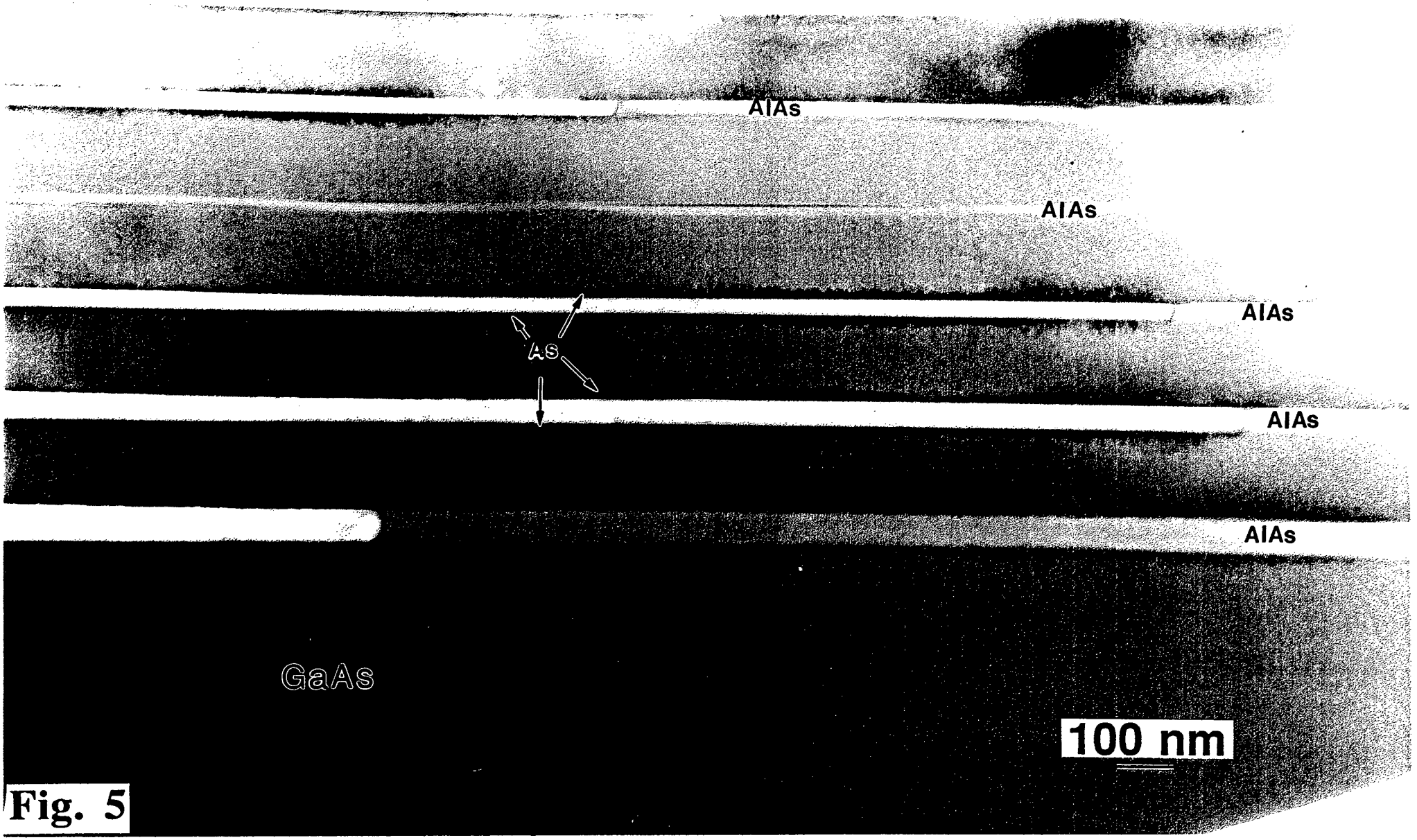

Fig. 5

Z. LILIENTAL-WEBER, LBNL, Berkeley, 1998

Fig. 6

Ż. LILIENTAL-WEBER, LBNL, Berkeley, 1998

Fig. 7

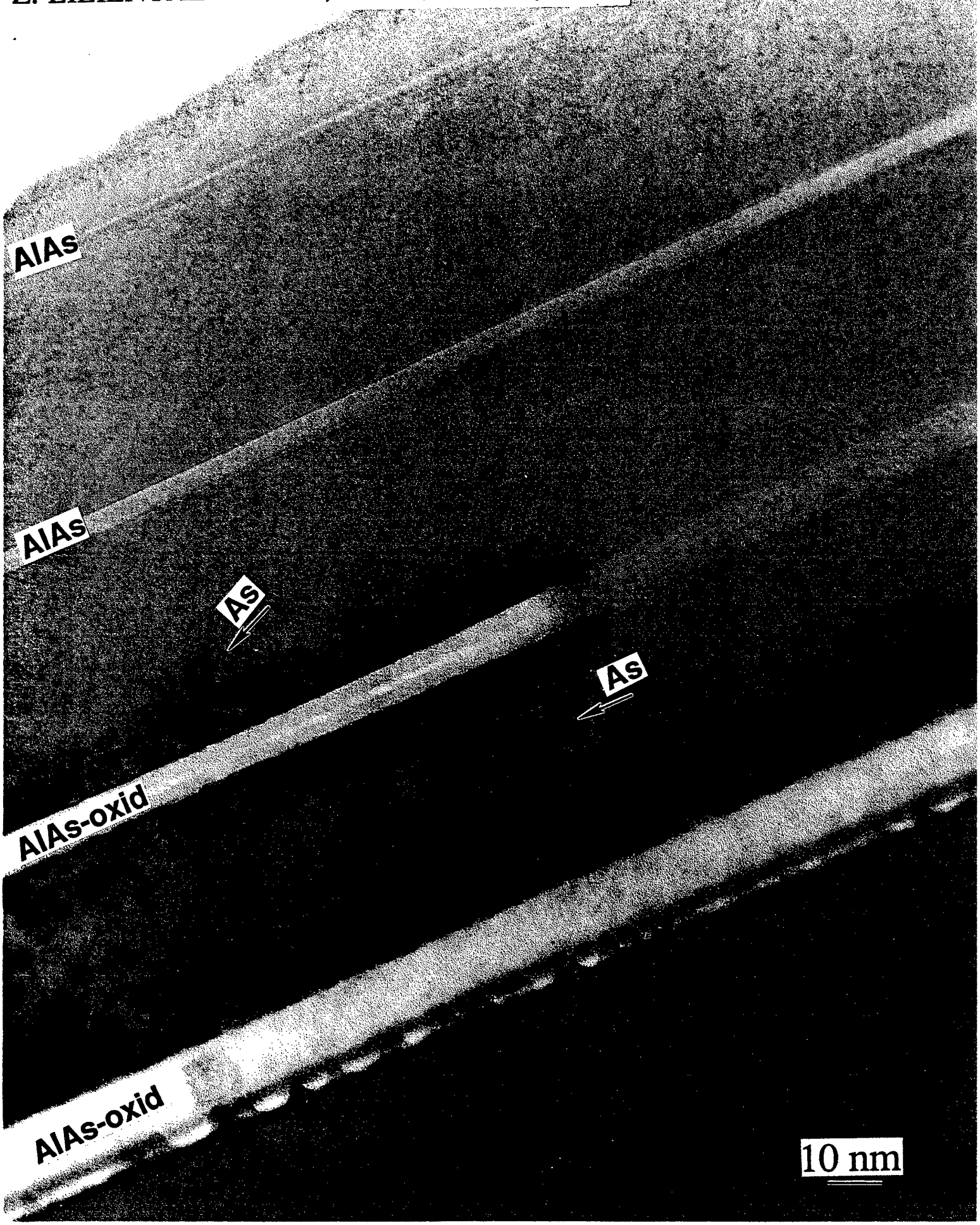

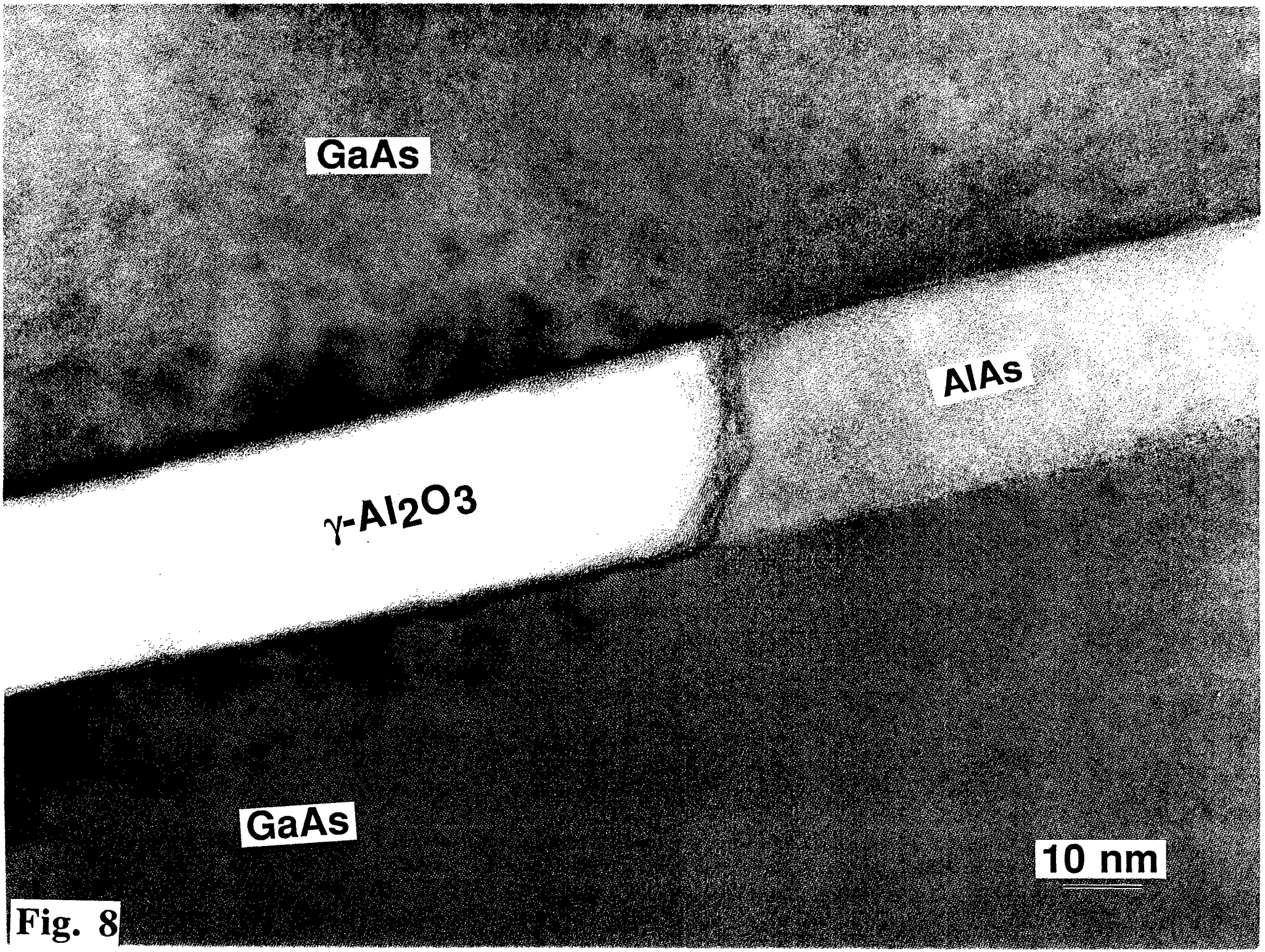

Fig. 8

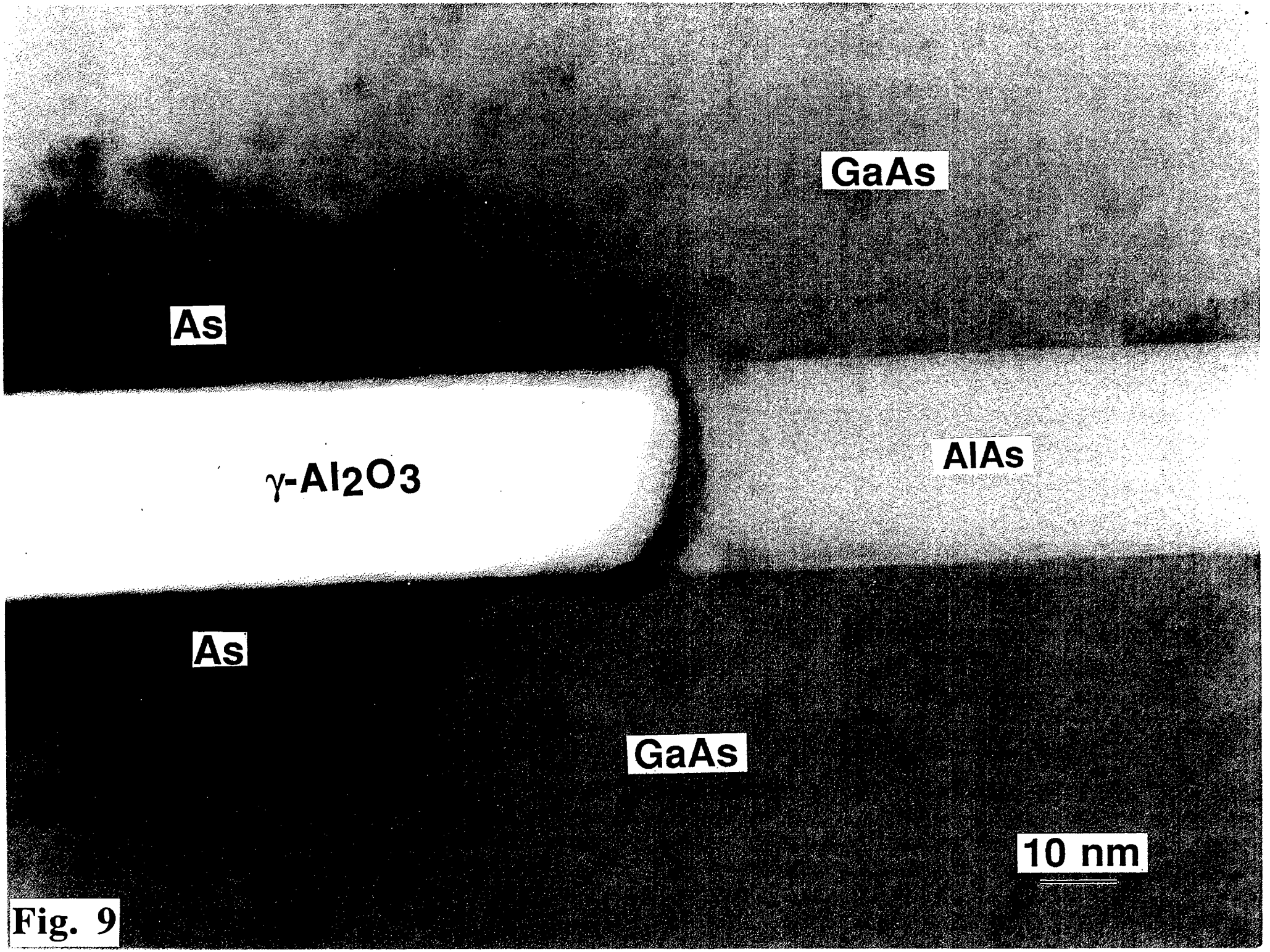

Fig. 9

Fig. 10

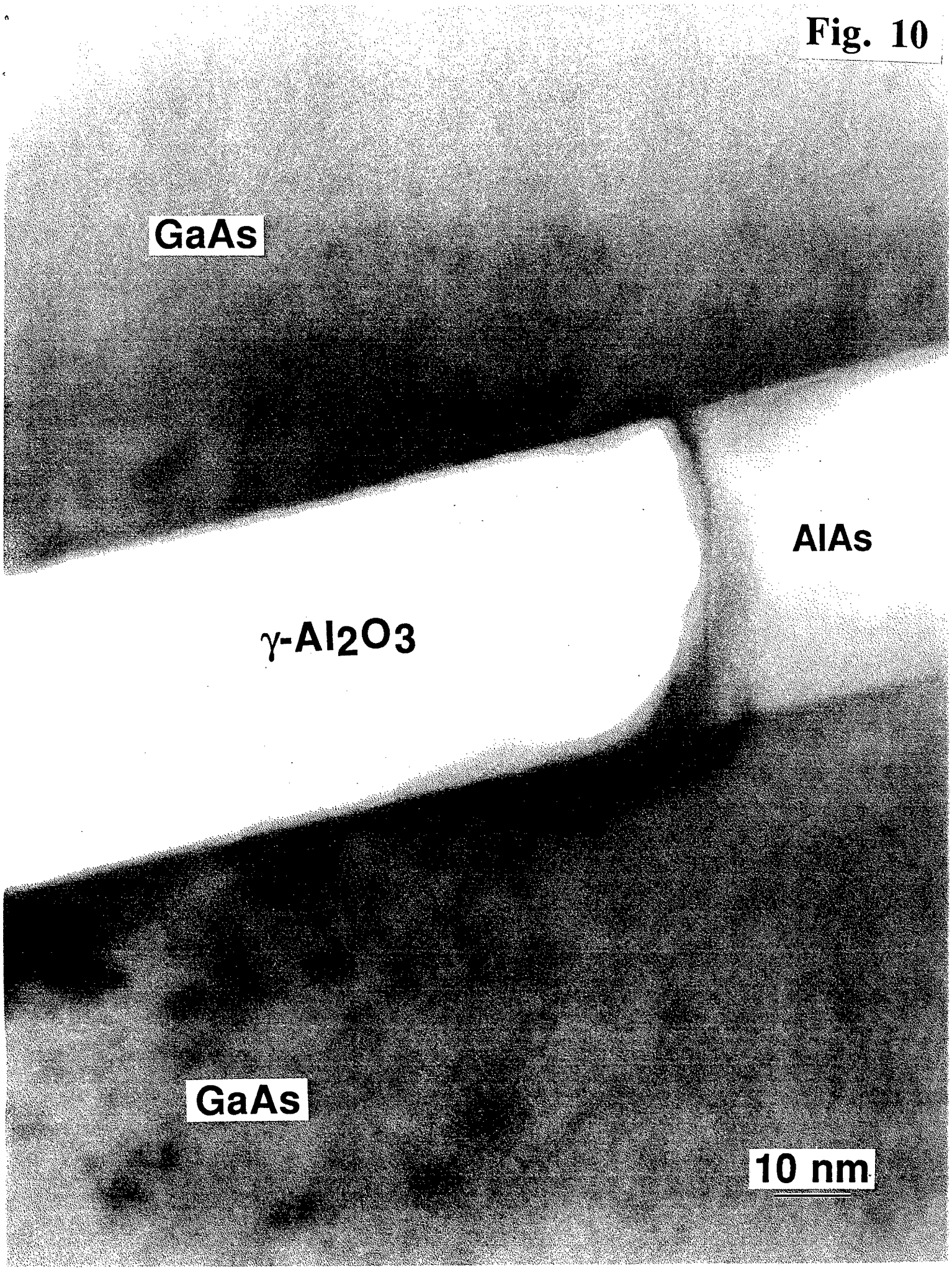

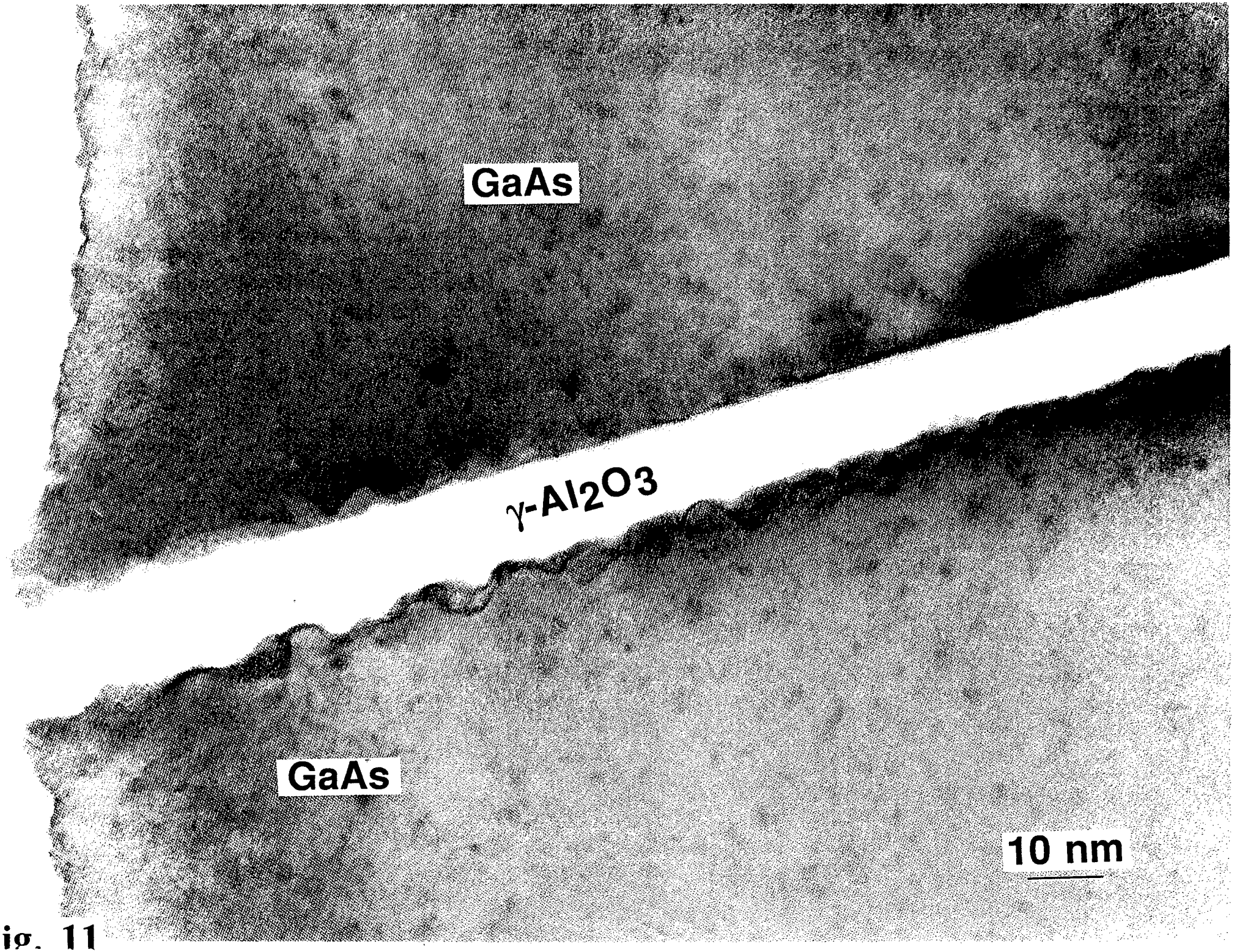

Fig. 11

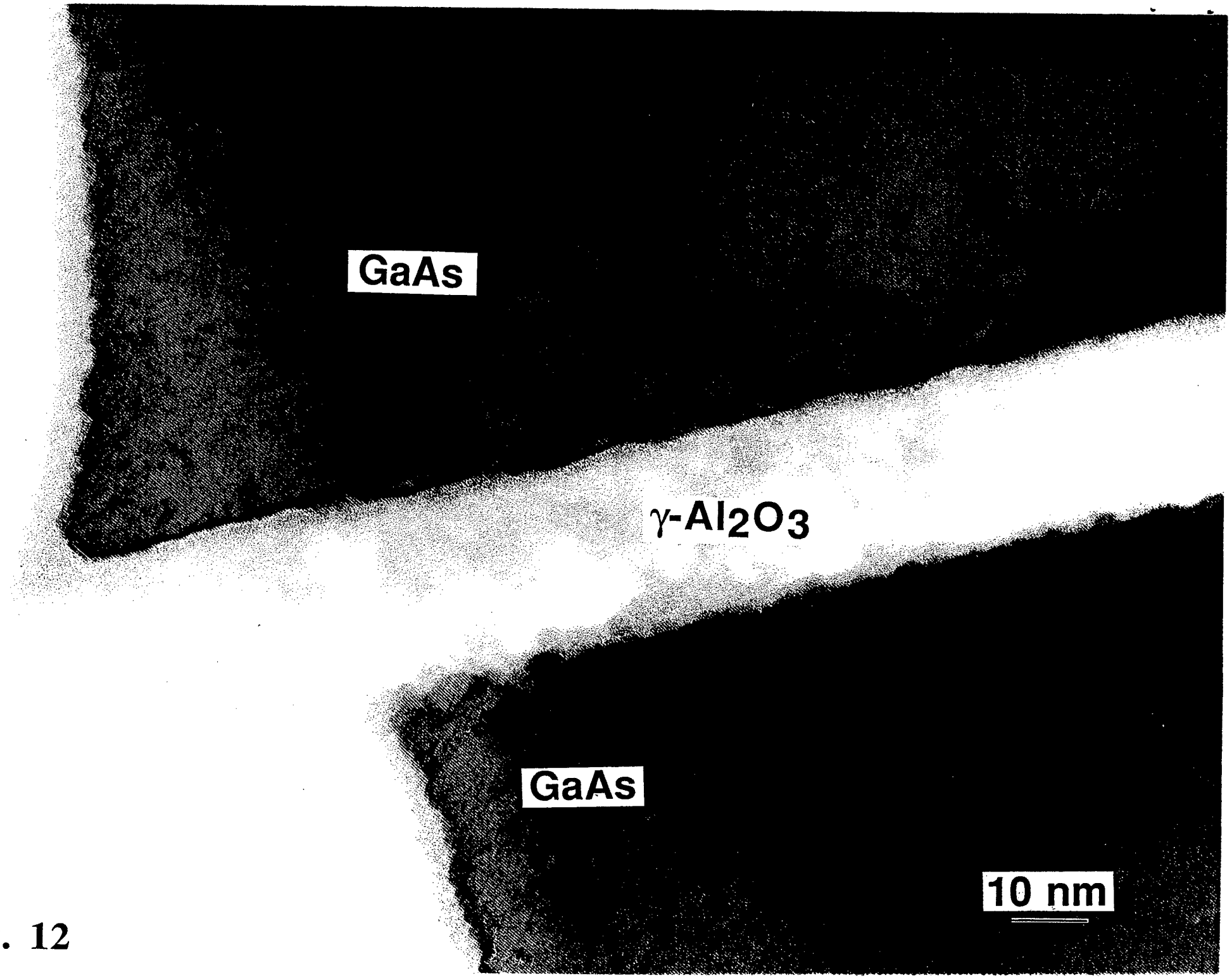

Fig. 12